Acta Crystallographica Section B
Structural Science
ISSN 0108-7681

Structure and oxygen mobility in mayenite ($Ca_{12}Al_{14}O_{33}$): a high-temperature neutron powder diffraction study

H. Boysen,[a]* M. Lerch,[b] A. Stys[b] and A. Senyshyn[c,d]

[a]Department für Geo- und Umweltwissenschaften, Sektion Kristallographie, LMU München, Am Coulombwall 1, 85748 Garching, Germany, [b]Institut für Chemie, TU Berlin, Strasse des 17 Juni 135, 10623 Berlin, Germany, [c]Materialwissenschaft, TU Darmstadt, Petersenstrasse 23, 64287 Darmstadt, Germany, and [d]FRM II, TU München, Lichtenbergstrasse 1, 85747 Garching, Germany

Correspondence e-mail: boysen@lmu.de

Received 17 January 2007
Accepted 19 June 2007

The structure of mayenite, $Ca_{12}Al_{14}O_{33}$, was investigated by neutron powder diffraction up to 1323 K. It has been described previously as a calcium–aluminate framework, in which 32 of the 33 oxygen anions are tightly bound, containing large cages, 1/6 of them being filled randomly by the remaining 'free' oxygen. At ambient temperature excess oxygen was found, corresponding to the composition $Ca_{12}Al_{14}O_{33.5}$ which was attributed to the presence of hydroxide, peroxide and superoxide radicals in the cages. Above 973 K these are lost under vacuum conditions and the composition becomes stoichiometric. From the refined structural parameters it is concluded that the structure is more adequately described as a relatively stable aluminate framework consisting of eightfold rings of AlO_4 tetrahedra with disordered Ca and 'free' O distributed within. At high temperatures the density of the 'free' oxygen is extremely spread out, with the expansion being related to the high ionic conductivity of this material. Since no continuous density distribution between adjacent cages was found and the 'free' O forms bonds with part of the Ca, the diffusion proceeds *via* a jump-like process involving exchange of the 'free' oxygen with framework oxygen. The results confirm the recent theoretical predictions of Sushko *et al.* [(2006), *Phys. Rev. B*, **73**, 014101-1-10].

1. Introduction

Mayenite ($Ca_{12}Al_{14}O_{33}$), known for a long time as a major constituent of calcium aluminate cements and discovered in 1964 as a mineral near Mayen, Eifel, Germany (Hentschel, 1964), has recently attracted much attention in materials sciences, *e.g.* as a transparent conductive oxide (TCO), as a catalyst for the combustion of volatile organic compounds or as an ionic conductor. At high temperatures a high oxygen ionic conductivity not far below that of yttria-stabilized zirconia (YSZ) was reported by Lacerda *et al.* (1988). It is also known that oxygen can be substituted selectively by other anions such as fluoride, chloride, hydroxide or hydride (Jeevaratnam, Glasser & Dent Glasser, 1964). More recently, electron anions have been incorporated (Matsuishi *et al.*, 2003), leading to the TCO properties of the material, and mayenite has been discussed as an inorganic electride (see *e.g.* Sushko *et al.*, 2003; Medvedeva & Freeman, 2004; Li *et al.*, 2004). Depending on the preparation conditions, the inclusion of superoxide O_2^- and O^- anions (Hosono & Abe, 1987; Hayashi *et al.*, 2002; Hayashi, Matsuishi, Hirano & Hosono, 2004; Hayashi, Ueda, Hirano & Hosono, 2004) and peroxide O_2^{2-} (Yang *et al.*, 2004) has also been reported, leading to oxygen excess, $Ca_{12}Al_{14}O_{33+\varepsilon}$, over the stoichiometric composition. These latter, highly reactive species are respon-

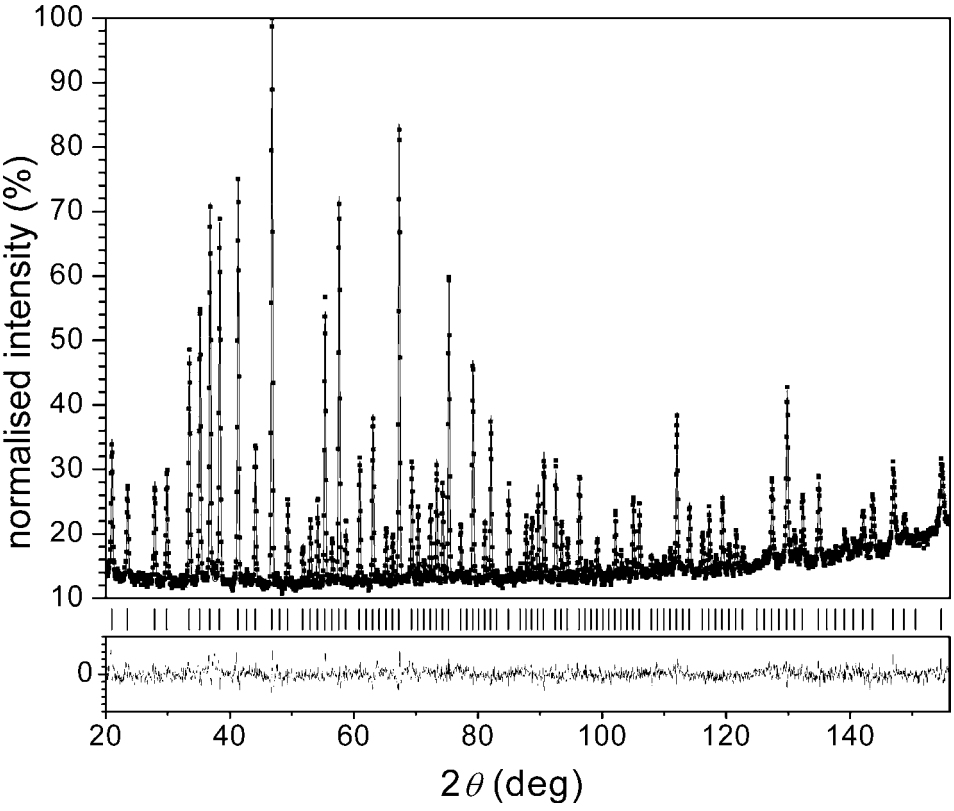

Figure 1
Observed (crosses) and calculated (solid line) powder pattern of mayenite at 973 K. The tick marks indicate the reflection positions. The difference plot is shown below.

sible for the catalytic activity. All these interesting properties have been related to the particular crystal structure, first determined by Büssem & Eitel (1936) and later refined by Bartl & Scheller (1970) and Christensen (1987). It is commonly described as a cubic nanoporous zeolite-like structure (space group $I\bar{4}3d$), containing two formula units per unit cell (a = 11.98 Å). There are 64 out of the 66 oxygen ions which are assumed to be fixed in a Ca–Al–O framework forming 12 'cages' per unit cell, 5–6 Å in diameter. The remaining two oxygen ions, termed 'free', 'extra-framework' or 'excess' oxygen, are statistically distributed inside 1/6 of the cages and may be exchanged by other anions, as mentioned above. The high mobility of these oxygen ions has been related to large 'windows' between these cages, ~3.7 Å in diameter. This simple view has recently been questioned by molecular dynamics and *ab initio* calculations by Sushko *et al.* (2006), which suggested that the

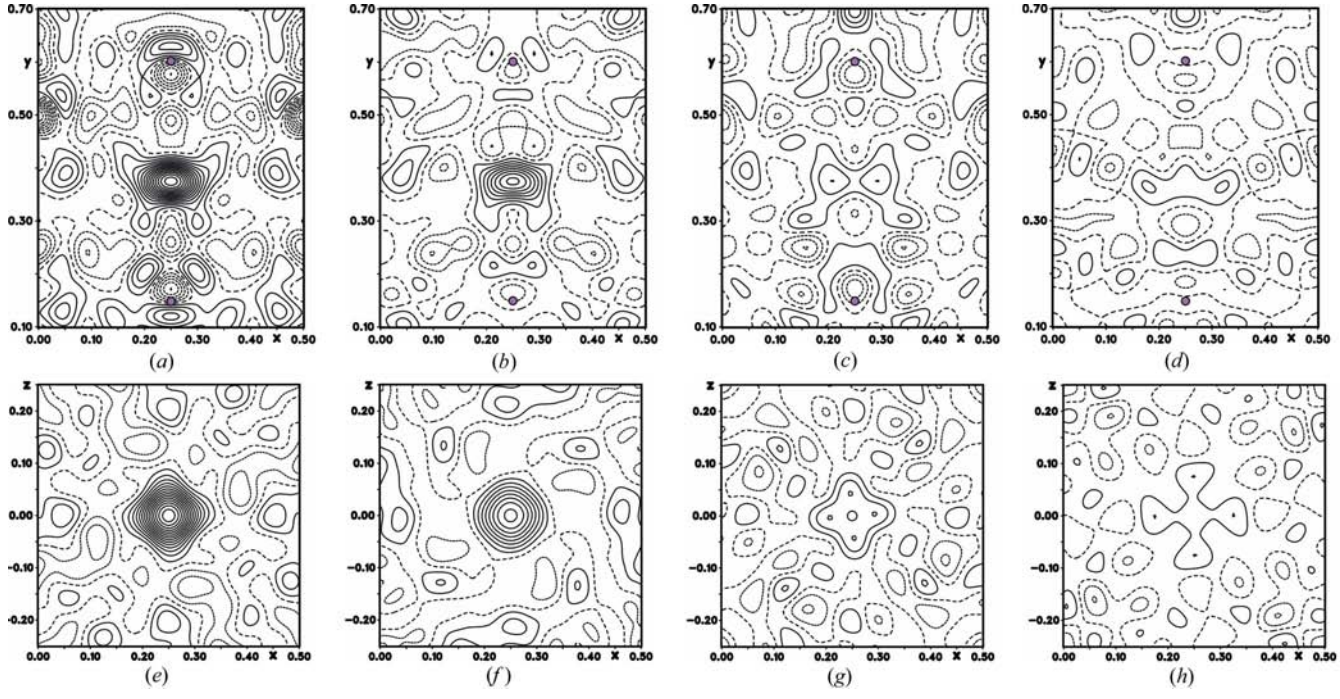

Figure 2
Difference-Fourier plots after refinement with framework atoms only at (*a*, *e*) 293, (*b*, *f*) 973, (*c*, *g*) 1173 and (*d*, *h*) 1323 K. The plots on the upper row show the *x y* 0 plane (with Ca ions marked by circles), those on the lower row perpendicular sections (*x* 3/8 *z*) through O3.

Table 1
Experimental details.

	(I)	(II)	(III)	(IV)
Crystal data				
Chemical formula	$Al_{14}Ca_{12}O_{33}$	$Al_{14}Ca_{12}O_{33}$	$Al_{14}Ca_{12}O_{33}$	$Al_{14}Ca_{12}O_{33}$
M_r	1386.7	1386.7	1386.7	1386.7
Cell setting, space group	Cubic, $I\bar{4}3d$	Cubic, $I\bar{4}3d$	Cubic, $I\bar{4}3d$	Cubic, $I\bar{4}3d$
Temperature (K)	298	973	1223	1323
a (Å)	11.9794	12.0308	12.0449	12.0585
V (Å^3)	1719.13	1741.32	1747.46	1753.40
Z	2	2	2	2
D_x (Mg m^{-3})	2.678	2.644	2.635	2.626
Radiation type	Neutron	Neutron	Neutron	Neutron
Specimen form, colour	Powder, white	Powder, white	Powder, white	Powder, white
Specimen size (mm)	8 mm diameter, 15 mm height	8 mm diameter, 15 mm height	8 mm diameter, 15 mm height	8 mm diameter, 15 mm height
Data collection				
Diffractometer	Debye–Scherrer	Debye–Scherrer	Debye–Scherrer	Debye–Scherrer
Data collection method	Specimen mounting: in V can; scan method: 2θ	Specimen mounting: in V can; scan method: 2θ	Specimen mounting: in V can; scan method: 2θ	Specimen mounting: in V can; scan method: 2θ
2θ (°)	$2\theta_{min}$ = 20.05, $2\theta_{max}$ = 139.950, increment = 0.05	$2\theta_{min}$ = 20.05, $2\theta_{max}$ = 155.950, increment = 0.05	$2\theta_{min}$ = 20.05, $2\theta_{max}$ = 151.950, increment = 0.05	$2\theta_{min}$ = 20.05, $2\theta_{max}$ = 151.950, increment = 0.05
Refinement				
R factors and goodness-of-fit	R_p = 0.026, R_{wp} = 0.034, R_{exp} = 0.020, S = 1.68	R_p = 0.030, R_{wp} = 0.039, R_{exp} = 0.028, S = 1.38	R_p = 0.030, R_{wp} = 0.040, R_{exp} = 0.025, S = 1.59	R_p = 0.034, R_{wp} = 0.045, R_{exp} = 0.031, S = 1.43
Wavelength of incident radiation (Å)	1.548	1.548	1.548	1.548
Excluded region(s)	0–20°	0–20°	0–20°	0–20°
Profile function	Pseudo-Voigt	Pseudo-Voigt	Pseudo-Voigt	Pseudo-Voigt
No. of parameters	45	41	42	41
Weighting scheme	Based on measured s.u.'s 102	Based on measured s.u.'s 102	Based on measured s.u.'s 102	Based on measured s.u.'s 401
$(\Delta/\sigma)_{max}$	0.018	0.020	0.041	0.017

Computer programs used: *JANA*2000 (Petricek *et al.*, 2000).

diffusion process is dominated by an exchange of framework and extra-framework ions. In order to determine the distribution of the 'free' oxygen ions and possible diffusion pathways in more detail we have performed a high-temperature neutron powder diffraction study up to 1323 K. Moreover, a critical discussion of the room-temperature structure as reported in the literature will be presented in light of our new measurements.

2. Experimental

Mayenite powder was synthesized by a solid-state route. CaO, prepared by the decomposition of $CaCO_3$ (99+, Alfa), was mixed with Al_2O_3 (purest, Merck) and dried at 453 K for 1 week. After homogenization in an agate mortar the mixture was heated in air at 1623 K for 24 h. After cooling down it was powdered and heated a second time for 48 h. XRD measurements revealed a pure mayenite phase. The hydrogen content of the sample was determined to 0.07 wt % by combustion analysis.

Elastic scattering experiments were carried out at the neutron powder diffractometer SPODI at the FRM II (Garching, Germany) equipped with 80 vertically position-sensitive ^{3}He detectors (Gilles *et al.*, 2002) at 298, 973, 1223 and 1323 K using a wavelength of 1.548 Å. The angular range 2θ = 0–160° was scanned with a step size of 0.05°. The quasi two-dimensional data set was corrected for efficiency and geometrical aberration which are intrinsic for each collimator–detector pair. Final powder patterns were obtained by integration along the Debye–Scherrer cones. The high-temperature measurements were performed using a vanadium container and a niobium vacuum furnace (*ca* 10^{-6} bar). Data analysis was performed with the Rietveld option of the program package *JANA*2000 (Petricek *et al.*, 2000) using Legendre polynomials as a description of the background and pseudo-Voigt profiles for the peak shapes. While the data reduction procedure strongly diminishes the asymmetry of the lines, the finite sample height leads to considerable deviations from the ideal pseudo-Voigt profile at low angles. Therefore, the first strong peak below 20° was excluded from the fit. As an example of the goodness of the final fits, the observed and calculated powder diffraction patterns at 973 K are shown in Fig. 1. Experimental details are given in Table 1.[1]

3. Results

In a first step structure refinements have been performed with only the framework atoms (including anisotropic atomic displacement parameters, ADPs), in order to reveal the

[1] Supplementary data for this paper are available from the IUCr electronic archives (Reference: WS5057). Services for accessing these data are described at the back of the journal.

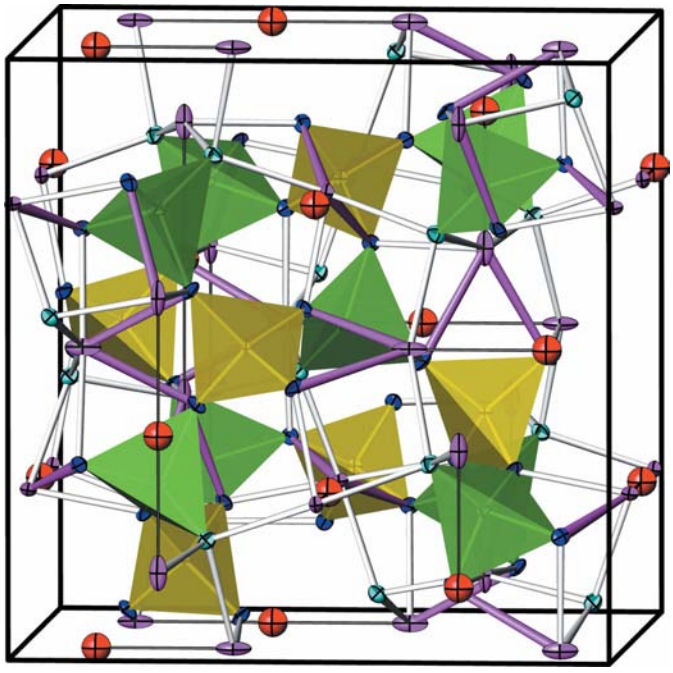

Figure 3
Structure of mayenite at 293 K with atoms represented by ADP ellipsoids. $Al1O_4$ and $Al2O_4$ tetrahedra are shown in dark (green) and light (yellow), respectively, O1 and O2 in dark (blue) and light (cyan). Ca (purple) may be recognized by strongly elongated ellipsoids and O3 (red) by large spheres. 'Normal' and 'large' Ca—O bonds are discriminated by thin light and thick dark (purple) lines, respectively. Ca and O3 are connected by thin black lines.

location of the extra-framework oxygen O3 by difference-Fourier methods. The results for all temperatures are shown in Fig. 2. As seen, O3 is clearly located at the centre of the cage in a 12(*a*) $\frac{1}{4}, \frac{3}{8}, 0$ position with $\bar{4}$ site symmetry. This is in clear contrast with the split 24(*d*) $\frac{1}{4}, y, 0$ position reported by Bartl & Scheller (1970) and generally accepted in the literature. Note that this splitting would be in the *y* direction in Fig. 2 (top-row drawings). Test refinements with this split position were unstable (trying to shift the *y* parameter towards $\frac{3}{8}$), *i.e.* this can be firmly excluded at least for our sample. On the other hand, there are indications of displacements in *x*,*z* directions [general 48(*e*) position, see the pronounced lobes on the lower-row drawings in Fig. 2]. It should be noted that these lobes are far less pronounced at 973 K and that the overall scattering density strongly decreases between room temperature and 973 K, and becomes very much spread out at the higher temperatures. In a next step O3 was introduced into the refinements with isotropic ADPs. At room temperature, apart from O3 and also Ca, all the positional and displacement parameters of the framework atoms are in good agreement with the literature values. The resulting structure also showing the ADP ellipsoids is depicted in Fig. 3. Al forms fairly regular AlO_4 tetrahedra (see Table 2), partly interconnected by common corners to build eightfold rings and partly *via* bridging Ca. The rather irregular Ca polyhedron has four 'normal' bonds (2.35 and 2.39 Å) in an almost planar configuration and two 'too' long bonds (2.59 Å) which are not much smaller than that to O3 (2.73 Å). The two 'long' bonds are connected to the $Al2O_4$ tetrahedron with the apex (Ca) pointing towards O3. Together with the remarkable anisotropy of the ADP ellipsoid of Ca in the same direction, this points to a considerable disorder of Ca.

The lattice constants show a nearly linear increase with temperature (Fig. 4) with a linear thermal expansion coefficient of 6.36 (1) $\times 10^{-6}$ K^{-1}. This value is considerably larger than that reported by Datta (1987), 4. 1 $\times 10^{-6}$ K^{-1}, for samples prepared from the melt, but agrees with values for samples prepared through solid-state reaction below 1573 K, as cited by Datta. While the ADPs of Al also behave normally, increasing linearly with temperature, those of Ca and the framework O are pronouncedly non-linear (Fig. 5). The large intercepts at 0 K can certainly not be attributed to zero-point motions and therefore confirm the very large static disorder component of Ca, and also some disorder of framework O, in contrast to only the small component of Al. As seen in Fig. 6 there is a striking anomaly of the isotropic ADPs of O3, which

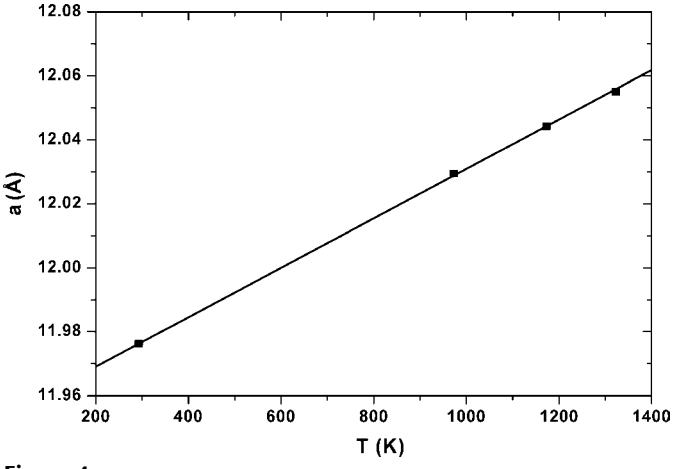

Figure 4
Thermal expansion of mayenite (error bars are smaller than the symbols).

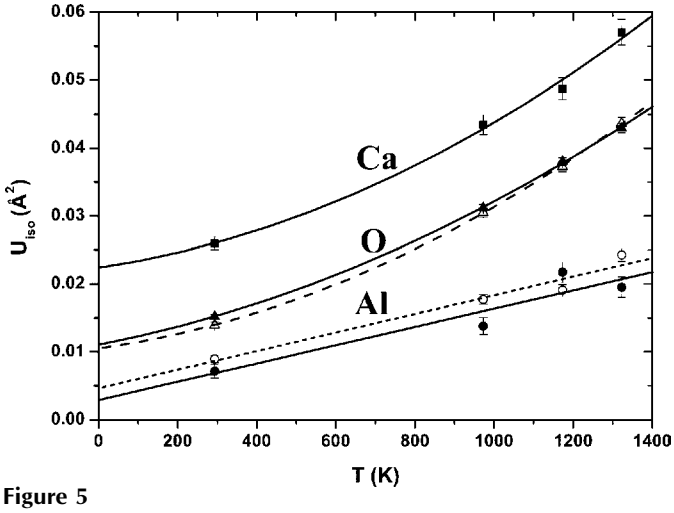

Figure 5
Temperature variation of (equivalent) isotropic ADPs of framework atoms after refinement without split Ca′ (*i.e.* not the final refinement, see text). O1 and O2 as well as Al1 and Al2 are shown as open and solid symbols, respectively.

Table 2
Selected bond lengths (Å).

T (K)	293	973	1173	1323
Ca—O1 (2×)	2.354 (1)	2.372 (2)	2.379 (2)	2.390 (2)
Ca—O1 (2×)	2.556 (3)	2.603 (4)	2.605 (5)	2.611 (6)
Ca—O2 (2×)	2.404 (2)	2.407 (2)	2.421 (2)	2.421 (2)
Ca—O3	2.777 (4)	2.750 (5)	2.768 (6)	2.766 (7)
Ca—Ca′	0.52 (2)	0.59 (3)	0.79 (6)	0.80 (9)
Al1—O1 (3×)	1.775 (2)	1.781 (3)	1.778 (3)	1.774 (4)
Al1—O2	1.734 (2)	1.712 (3)	1.718 (3)	1.718 (4)
Al2—O1 (4×)	1.734 (1)	1.744 (2)	1.739 (2)	1.741 (2)
Ca′—O1 (2×)	2.392 (6)	2.434 (8)	2.489 (16)	2.51 (3)
Ca′—O2 (2×)	2.351 (1)	2.365 (2)	2.388 (7)	2.39 (1)
Ca′—O3	2.26 (2)	2.16 (3)	1.98 (6)	1.96 (9)

become extremely large at the two highest temperatures. This is accompanied by a strong temperature dependence of the occupancies of O3 (Fig. 7), being far too large at room temperature and roughly in agreement with the nominal stoichiometry (horizontal line in Fig. 7) at 973 K and above. All these and further features of the difference-Fourier maps (Fig. 2) can be explained by the presence of peroxide and/or superoxide and hydroxide anions at room temperature, their loss at 973 K and the increasing mobility of the O3 anions at higher temperatures, as will be discussed separately below. Final refinements included the isotropic ADP for O3 and an additional split position for Ca imposed by the strong static disorder component as anticipated above. These split (Ca′) positions may be derived from the location of the residual peaks in the difference-Fourier maps near Ca in Fig. 2, and, more clearly in a further difference-Fourier map after inclusion of O3 at 973 K (Fig. 8). They appear to be displaced mainly along [010] towards O3, but shifted somewhat sideward perpendicular to [010], *i.e.* in a general 48(*e*) position. Since, however, for both O3 and Ca′, a further sideward splitting as suggested by the difference-Fourier maps did not lead to stable refinements because of strong correlations, and anisotropic ADPs to mimic the further splitting were not always positive definite, Ca′ was put on a 24(*d*) (x 0 $\frac{1}{4}$) position and only isotropic ADPs were used for these two atoms. The resulting occupancies of Ca and Ca′ always added up to the full Ca content given by the stoichiometry within one standard deviation. Moreover, it is tempting to assume that the Ca′ position, shifted towards the centre of the cage, is occupied only if that cage is occupied by O3 at the same time. This was suggested by the theoretical work of Sushko *et al.* (2006) and has in fact already been found much earlier in the fluorinated analogue by Williams (1973). Although with free refinements of their occupancies this condition was fulfilled only within two (large) standard deviations, they were constrained to the conditions n(O3) = n(Ca′) = 0.5 − n(Ca), in order to reduce the correlations with the ADPs. All final refined parameters are given in the supplementary material and selected bond lengths in Table 2.

4. Discussion

4.1. The mayenite structure at room temperature

The refined occupancy of O3 means an excess over the stoichiometric composition, at $Ca_{12}Al_{14}O_{33.53}$. This value is in good agreement with the literature, *e.g.* Trofymluk *et al.* (2005) report a composition of $Ca_{12}Al_{14}O_{33.46}$ as being the 'most stable'. As widely discussed in the literature, this excess may be attributed to the presence of OH^-, O_2^-, O_2^{2-} or O^- anions. To identify the actual species in our case, further difference Fourier analyses after the inclusion of (isotropic) O3 at 12(*a*) and the split Ca′ cation at 24(*d*) have been performed. Fig. 9(*a*) shows a section through the cage around O3. As seen in Fig. 9(*b*) this cage roughly has the form of a flattened rotational ellipsoid with the short extension (∼ 5.4 Å) defined by two Ca ions along the $\bar{4}$ axis and two long axes of ∼ 6.6 Å. In the immediate neighbourhood of O3 there are two positive and two negative peaks. The positive ones have a distance of ∼ 1.5 Å (indicated by the arrow in Fig. 9*a*), which would correspond to the O—O distance in peroxide anions O_2^{2-}. The negative ones (indicated by crosses in Fig. 9*a*) have a distance of ∼ 0.9 Å from O3, corresponding to the O—H distance in

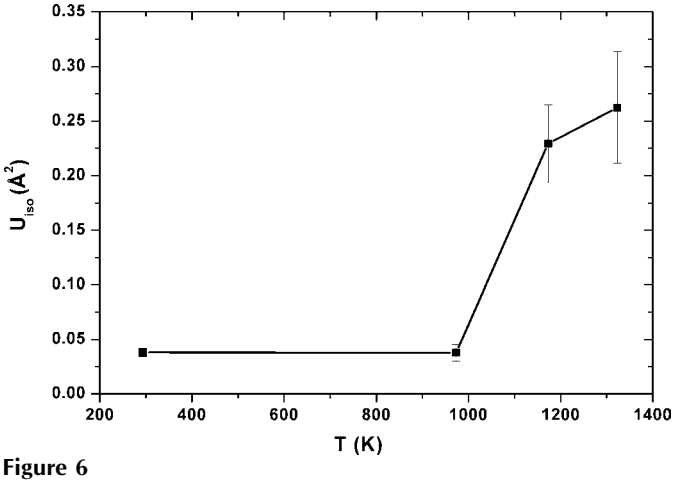

Figure 6
Temperature variation of isotropic ADP of 'free' oxygen O3 after refinement without Ca′.

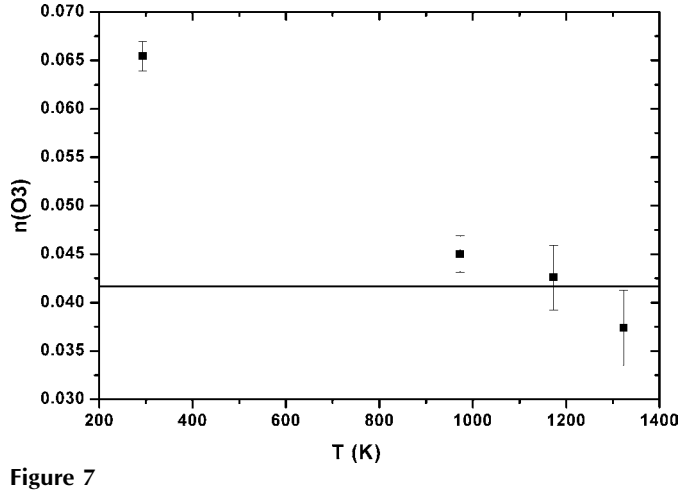

Figure 7
Temperature variation of the occupancy of 'free' oxygen O3 after refinement without Ca′ and special constraints (see text). The horizontal line indicates the expected occupancy for stoichiometric $Ca_{12}Al_{14}O_{32}$ O.

hydroxide anions OH^- (note that hydrogen has a negative scattering length for neutrons). In spite of the presence of many more residual peaks in the difference-Fourier maps, from these good agreements one may be confident that both species are indeed present in our sample and readily explain the excess occupancy of O3. The amount of H determined experimentally (0.07 wt %), assumed to be present as OH^- only, leads to the composition $O_{33.5}H$, which would be in excellent agreement with the refined O3 occupancy. However, this coincidence should be viewed with some care regarding the strong correlations between occupancy and ADP (approximated isotropic only) of O3, *i.e.* it does not rule out the presence of other anions. Further support for the loss of hydrogen at 973 K comes from the observation of a large reduction of the background in the powder patterns (related to the large incoherent scattering cross section of H) upon heating. The nearly 'correct' occupancy at 973 K is in agreement with various reports in the literature that both types of anions are lost approximately at this temperature (*e.g.* Hayashi, Matsuishi, Hirano & Hosono, 2004; Hayashi *et al.*, 2005). It is also noteworthy that the O_2^{2-} groups are oriented along the large extension of the cage, while the OH^- groups point towards Ca^{2+}. It has to be kept in mind, however, that, according to the literature, O_2^- and O^- anions may also be present, but are probably hidden within the density distribution of the actual O^{2-} anions, and that O^- and O^{2-} may adopt off-centre positions (see below) in the cage. A number of test refinements have been undertaken to include these species, partly supporting our conclusions. Unfortunately, however, the multitude of possible atoms, narrowly spaced around the O3 position in the average structure, lead to very strong correlation between the occupancies, ADPs and positions resulting in very large errors, not allowing any definite quantitative conclusion. Powder methods are certainly at their limits to reveal such fine details.

4.2. The mayenite structure at 973 K

Since the room-temperature structure was contaminated by the included anions other than O^{2-}, we discuss the proper structure of stoichiometric mayenite at 973 K, where O3 is still well located at the centre of the cage on the 12(*a*) position with a not too large and more isotropic ADP and has a 'correct' value of its occupancy. The slight excess still present at this temperature (Fig. 7, see supplementary material) may be due to a few remaining other species, but may be neglected for the following discussion. As mentioned, the shifts of Ca ions towards O3 were recently predicted by theoretical calculations of various authors, first for mayenite containing electrons (*e.g.* Sushko *et al.*, 2003), but also for the proper O^{2-}-containing mayenite (*e.g.* Li *et al.*, 2004). Sushko *et al.* (2006) report a displacement of ~ 1 Å, which is somewhat larger than the value found here (0.6 Å, Table 2), but taking into account that the proper Ca′ positions are displaced somewhat sideward as argued above (thus increasing the Ca—Ca′ distance), our result nicely confirms the theoretical calculations. Ca′ adopts a fivefold coordination with four 'normal' bond distances of ~ 2.4 Å to O1 and O2, respectively, and an apparently slightly too-short distance of ~ 2.2 Å to O3 (see Table 2). The latter may again be rationalized by the sideward displacements of Ca′ and also of O3 (more clearly seen at higher temperatures, see below) enlarging this distance to 'normal' values. Hence, the 'free' oxygen forms bonds with the displaced calcium.

As a consequence, the mayenite structure should be considered as a heavily disordered one, as regards both O3 and Ca′. This disorder may be envisaged as propagating along ...Ca—O3–Ca–Al2$O1_4$–Ca–O3–Ca... chains in ⟨100⟩ directions (see Fig. 3). Fig. 10 shows this chain using the ADPs of the highest measured temperature (1323 K) to enhance the displacement ellipsoids of all atoms. The O1 ellipsoids are strongly anisotropic roughly perpendicular to their bonds with Al2 (in the centre of the figure), trying to reduce the bonds which are too long to the adjacent Ca ions, whose ellipsoids are still elongated into the chain direction. Since the Al2—O1 bond lengths are independent of temperature and have a 'normal' value of 1.74 Å (see Table 2), the disorder is mainly connected with rotations of these tetrahedra. Consequently, a splitting of oxygen ions should also be expected, in agreement with their static disorder component derived above (Fig. 5). Moreover, the walls of occupied cages should be distorted. Although the difference-Fourier calculations gave some indication of the corresponding further split positions, their significance was too low to warrant any further detailed discussion.

4.3. The mayenite structure at high temperatures

As already seen in Figs. 2 and 6, the density of the 'free' oxygen O3 becomes extremely spread out at the two highest temperatures, indicating its large mobility certainly connected

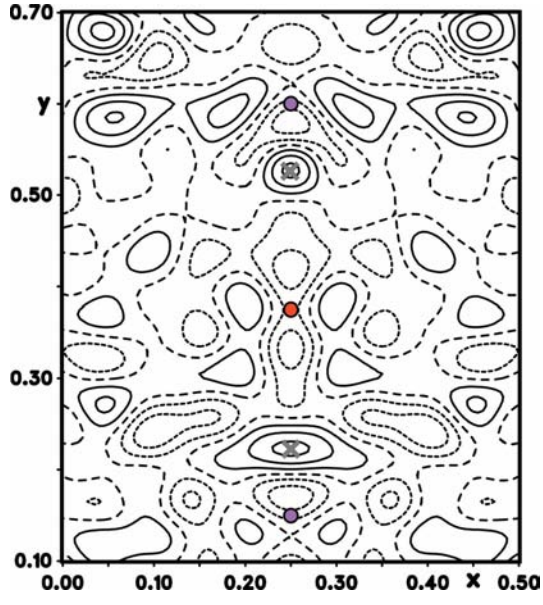

Figure 8
Difference-Fourier map after inclusion of O3 at 973 K (*cf.* Fig. 2*b*). The residual densities marked by crosses are attributed to split Ca positions (Ca′).

with ionic conduction. The final refined values of the occupancies and unrealistically large ADPs (supplementary material) can of course no longer be interpreted quantitatively. With regard to this, first attempts have been made to include anharmonic terms in the Debye–Waller factor to reveal the diffusion pathways and single particle potentials as is often successful in other cases of ionic conductors (Boysen, 2003). However, no significant results could be obtained probably because of an overall density of O3 which is too small in the average structure. On the other hand, this approach will not be successful if the diffusion does not proceed *via* an interstitial process with a continuous density distribution, but *via* a site-exchange process with local metastable positions as predicted by Sushko *et al.* (2006). Supporting evidence for the latter possibility comes from further difference-Fourier plots (after inclusion of O3 and Ca′), as shown *e.g.* in Fig. 11. The side maxima marked by crosses may be regarded as the true equilibrium positions of O3, in agreement with Sushko *et al.* (2006), that it adopts an off-centre position. As seen in Fig. 2 these off-centre shifts increase with increasing temperature. The general displacement direction is roughly the same as that predicted by Sushko *et al.* (2006), but the exact position appears to be slightly different as estimated from their Fig. 7. As anticipated above this position leads to a bond-like O3—Ca′ distance of 2.4 Å (note that the Ca′ shifts also increase with temperature, see supplementary material). It is then tempting to regard the band of positive density towards the peak marked by a star in Fig. 11(*b*) as a possible diffusion path. The latter (starred) maximum is close to a fourfold ring of the cage wall (*cf.* Fig. 9*b*) made up of Al1 (at a distance of 1.7 Å), Ca or Ca′ (at 2.1 Å) and two O1 (at 1.3 and 1.8 Å, respectively), *i.e.* it may represent a metastable position of O3 bonded to Al1 and Ca. Again this is similar although not exactly the same as in the calculations of Sushko *et al.* (2006), *cf.* their Fig. 8, indicating a site-exchange process of O3 with O1 of the Al1 tetrahedron. It is to be noted of course that this interpretation is fairly tentative with respect to the significance of our powder results since there are many more residual peaks, and only part of them can be interpreted in a similar way. Nevertheless, the important point is that there is no appreciable density near the centre of the sixfold rings made up of Ca/Ca′—O1—Al2—O1—Al1—O2 (*cf.* Fig. 9*b*), as revealed by further difference-Fourier calculations (not shown). This is in contrast to the previous literature (*e.g.* Lacerda *et al.*, 1988; Trofymluk *et al.*, 2005), where these rings were taken to be the 'large openings' through which the 'free' oxygen moves.

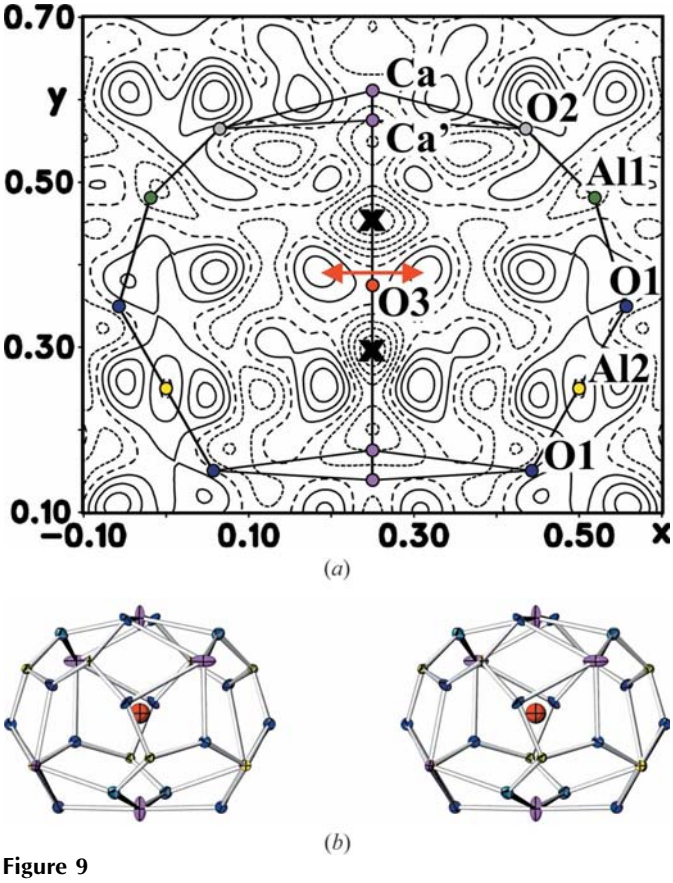

Figure 9
Difference-Fourier plot of a section (*xy*0) through the cage surrounding an O3 position after inclusion of (isotropic) O3 and Ca′ at room temperature (*a*). Al and O atoms lie above and below this plane, as illustrated by the stereo pair of the cage (without Ca′ for clarity) in (*b*). The arrow in (*a*) indicates the assumed O_2^{2-} species, the crosses indicate the H^+ positions (having negative scattering length) associated with the assumed OH^- species.

5. Conclusions

Without taking special precautions in their preparation, mayenite samples contain various additional anions such as peroxide, superoxide and hydroxide at room temperature, leading to an excess over the stoichiometric composition. Under vacuum conditions these extra anions are lost with increasing temperatures. Above 973 K the ideal composition, $Ca_{12}Al_{14}O_{33}$, is adopted. The mayenite structure possesses a relatively stable framework of AlO_4 tetrahedra forming eightfold rings as evidenced by the only marginal variations with temperature (see Table 2 and supplementary material). In this sense it should be regarded as consisting of an aluminate framework instead of a calcium-aluminate framework, as often claimed in the literature. It is heavily disordered with respect to extra-framework oxygen and calcium being

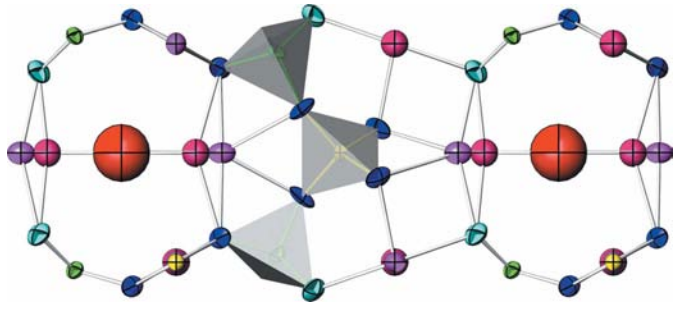

Figure 10
Two cages along the ⟨100⟩ direction connected *via* an $Al2O1_4$ tetrahedron in the centre at 1323 K. Large spheres are O3, small spheres and ellipsoids on the middle line are Ca′ and Ca, respectively.

distributed randomly in the aluminate framework, but probably with some chain-like short-range order. Normal bond lengths between the latter, similar to those in CaO, suggest that the 'free' oxygen is closely connected with Ca. This suggests a jump-like diffusion process involving both O and Ca at higher temperatures, where the extra-framework oxygen anions are widely spread out in line with the large ionic conductivity. Our results support the view of Sushko *et al.* (2006) that oxygen diffusion proceeds *via* site-exchange processes with framework oxygen.

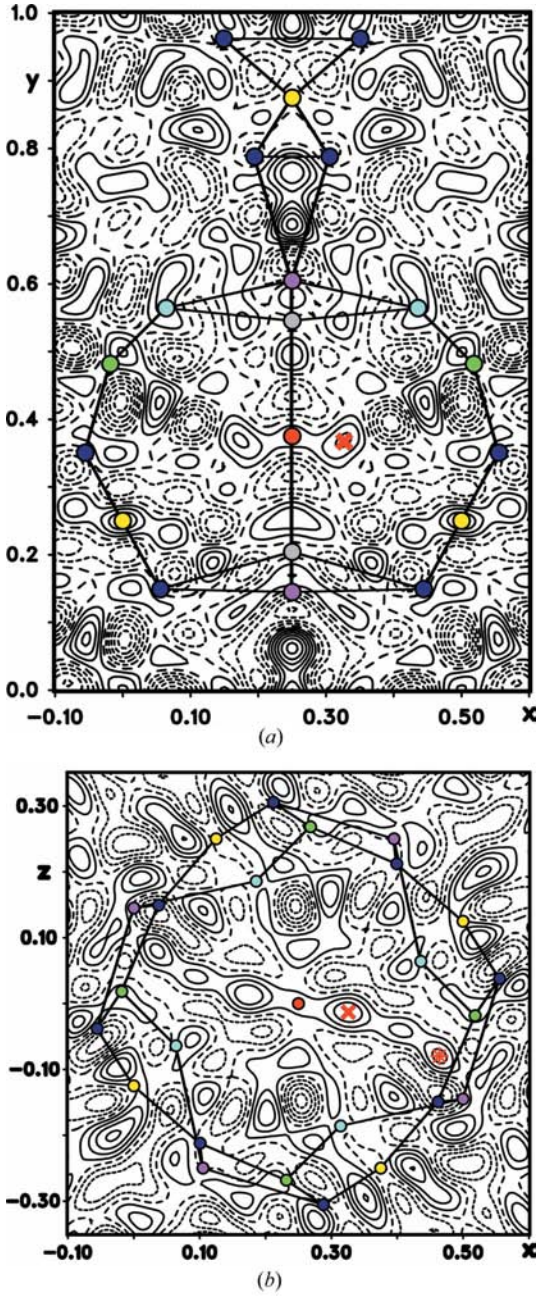

Figure 11
Difference-Fourier plot of an *xy*0 section (*a*) through the cage surrounding an O3 position with an adjacent $Al2O1_4$ tetrahedron at 1323 K and perpendicular *x* 0.385 *z* section (*b*) slightly above the O3 position to reach the maxima of the side peaks of O3. In (*b*) the fourfold (Ca–O1–Al1–O1) and sixfold (Ca–O2–Al1–O1–Al2–O1) rings of the cage wall are indicated (note that these are located partly significantly above and below the plane shown, *cf.* Fig. 9*b*), and Ca′ has been neglected for clarity. The peaks marked by crosses and a star are discussed in the text.

Finally, it has to be remarked that all the results presented in this paper may apply only for the specific sample used in this work, *i.e.* prepared by solid-state synthesis below 1623 K, and the measuring conditions, *i.e.* under vacuum. It is well known from the literature that different preparation and atmospheric environment conditions can lead to largely different results, with regard, for example, to the thermal expansion (Datta, 1987), the ionic conductivity (Matsuda *et al.*, 1996) and many other properties. All this must have a structural origin and it would therefore be highly interesting to perform analogous investigations under various other conditions to finally understand the peculiar behaviour of mayenite.

This work was supported by the DFG within the priority program SPP 1136 under BO 1199/2 and LE 781/10.

References

Bartl, H. & Scheller, T. (1970). *Neues Jahrb. Miner. Monatsh.* **35**, 547–552.
Boysen, H. (2003). *Z. Kristallogr.* **218**, 123–131.
Büssem, W. & Eitel, A. (1936). *Z. Kristallogr.* **95**, 175–188.
Christensen, A. N. (1987). *Acta Chem. Scand. A*, **41**, 110–112.
Datta, R. K. (1987). *J. Am. Chem. Soc.* **70**, C288–C291.
Gilles, R., Krimmer, B., Boysen, H. & Fuess, H. (2002). *Appl. Phys. A*, **74**, 148.
Hayashi, K., Hirano, M. & Hosono, H. (2005). *Chem. Lett.* **34**, 586–587.
Hayashi, K., Hirano, M., Matsuishi, S. & Hosono, H. (2002). *J. Am. Chem. Soc.* **124**, 738–739.
Hayashi, K., Matsuishi, S., Hirano, M. & Hosono, H. (2004). *J. Phys. Chem. B*, **108**, 8920–8925.
Hayashi, K., Ueda, N., Hirano, M. & Hosono, H. (2004). *Solid State Ion.* **173**, 89–94.
Hentschel, G. (1964). *Neues Jahrb. Miner. Monatsh.* pp. 22–29.
Hosono, H. & Abe, Y. (1987). *Inorg. Chem.* **26**, 1192–1195.
Jeevaratnam, J., Glasser, F. P. & Dent Glasser, L. S. (1964). *J. Am. Ceram. Soc.* **47**, 105–106.
Lacerda, M., Irvine, J. T. S., Glasser, F. P. & West, A. R. (1988). *Nature*, **332**, 525–526.
Li, Z., Yang, J., Hou, J. G. & Zhu, Q. (2004). *Angew. Chem.* **43**, 6479–6482.
Matsuda, M., Inda, Y., Hisamatsu, W., Yamashita, K. & Umegaki, T. (1996). *J. Mater. Sci. Lett.* **15**, 933–934.
Matsuishi, S., Toda, Y., Miyakawa, M., Hayashi, K., Kamiya, T., Hirano, M., Tanaka, I. & Hosono, H. (2003). *Science*, **301**, 626–629.
Medvedeva, J. E. & Freeman, A. J. (2004). *Appl. Phys. Lett.* **85**, 955–957.
Petricek, V., Dusek, M. & Palatinus, L. (2000). *JANA*2000. Institute of Physics, Praha, Czech Republic.
Sushko, P. V., Shluger, A. L., Hayashi, K., Hirano, M. & Hosono, H. (2003). *Phys. Rev. Lett.* **91**, 126401-1-4.
Sushko, P. V., Shluger, A. L., Hayashi, K., Hirano, M. & Hosono, H. (2006). *Phys. Rev. B*, **73**, 014101-1-10.
Trofymluk, O., Toda, Y., Hosono, H. & Navrotsky, A. (2005). *Chem. Mater.* **17**, 5574–5579.
Williams, P. P. (1973). *Acta Cryst.* B**29**, 1550–1551.
Yang, S., Kondo, J. N., Hayashi, K., Hirano, M., Domen, K. & Hosono, H. (2004). *Chem. Mater.* **16**, 104–110.